

Diperovskite $(\text{NH}_4)_3\text{FeF}_6$ /Graphene Nanocomposites towards

Superior Na-Ion Storage

Zhanghui Hao,^a Masayoshi Fuji^{b,*} and Jisheng Zhou^{a,*}

a. State Key Laboratory of Chemical Resource Engineering, Beijing Key Laboratory of Electrochemical Process and Technology for Materials, Beijing University of Chemical Technology, Beijing 100029, P. R. China.

b. Advanced Ceramics Research Center, Nagoya Institute of Technology, 3-101-1, Honmachi, Tajimi, Gifu 507-0033, Japan

* Corresponding authors: zhoujs@mail.buct.edu.cn (J Zhou) fuji@nitech.ac.jp (M Fuji)

Supporting Data:

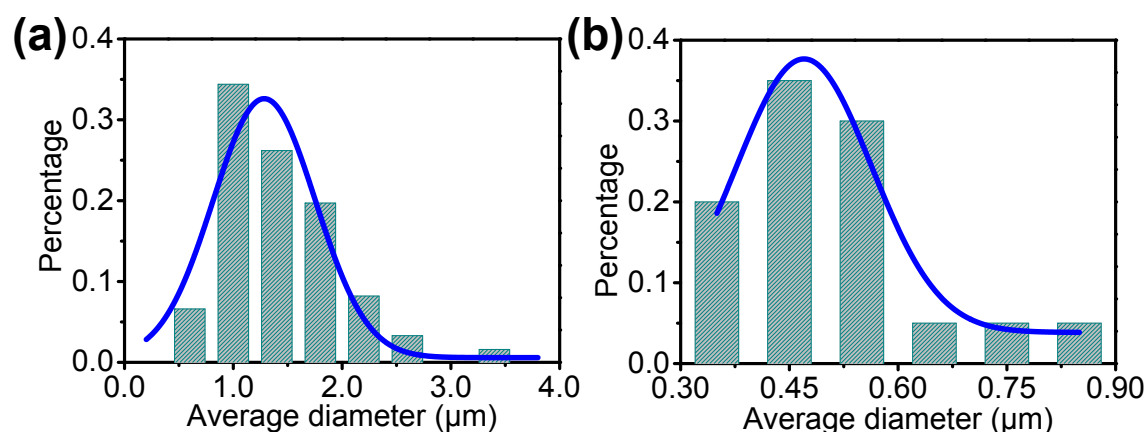


Figure S1. The particles size distribution of the (a) $(\text{NH}_4)_3\text{FeF}_6$ and (b) $(\text{NH}_4)_3\text{FeF}_6/\text{GNS}$ prepared at 200 °C for 2 h.

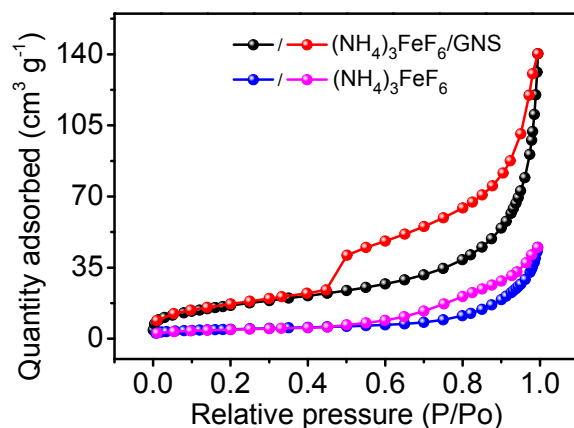


Figure S2. N₂ adsorption-desorption isotherms of the pure (NH₄)₃FeF₆ and (NH₄)₃FeF₆/GNS.

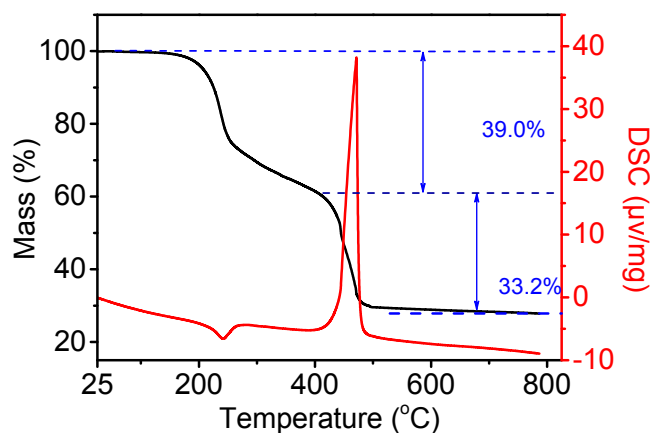


Figure S3. TG and DSC curves of the (NH₄)₃FeF₆/GNS obtained in air atmosphere from room temperature to 800 °C at a rate of 10 °C min⁻¹.

The TG curve of (NH₄)₃FeF₆/GNS can be divided into two stages: (I) at 25-400 °C, there is rapid weight loss of 39.0% at ca. 200 °C, which should be attributed to the transformation from (NH₄)₃FeF₆ phase to FeF₃ phase. There is an endothermic peak on the corresponding temperature range of differential scanning calorimetry (DSC) line; (II) at 400-800 °C, when the temperature up to 410 °C, the TG curve also display a rapid decline corresponding to the oxidations of graphene into CO₂/CO and FeF₃ into Fe₂O₃. Therefore, there is an obvious exothermic peak on the corresponding temperature range of DSC line. The (NH₄)₃FeF₆ and GNS content in (NH₄)₃FeF₆/GNS can be calculated to be ca. 78.0 wt% and 22.0 wt%, respectively.

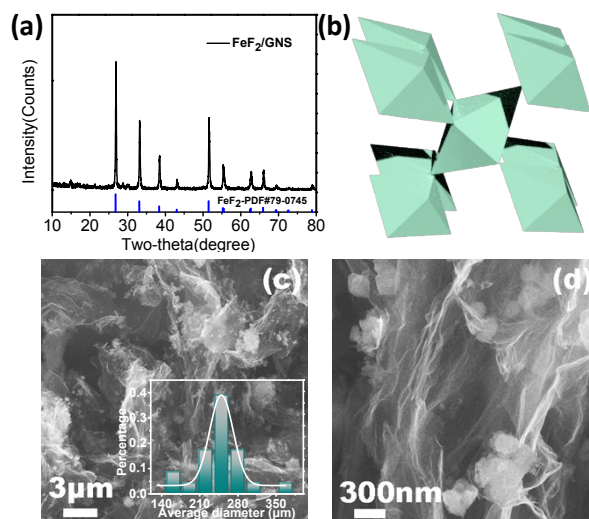


Figure S4. (a) XRD pattern, (b) crystal structure and (c, d) SEM images of FeF₂/GNS obtained by annealing (NH₄)₃FeF₆/GNS at 400 °C for 3 h.

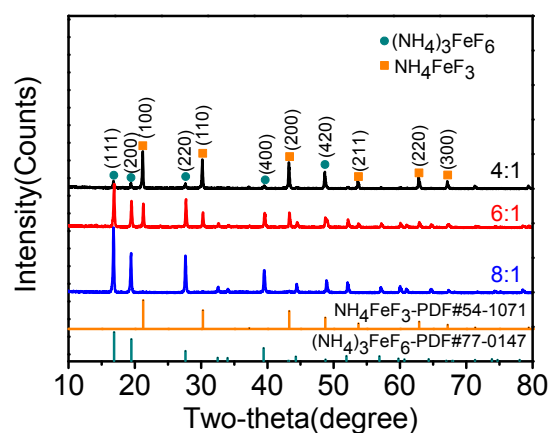


Figure S5. XRD pattern of the samples obtained at various $\text{NH}_4\text{F}/\text{Fe}(\text{acac})_3$ molar ratios of 4:1, 6:1 and 8:1 at 200 °C for 2 h.

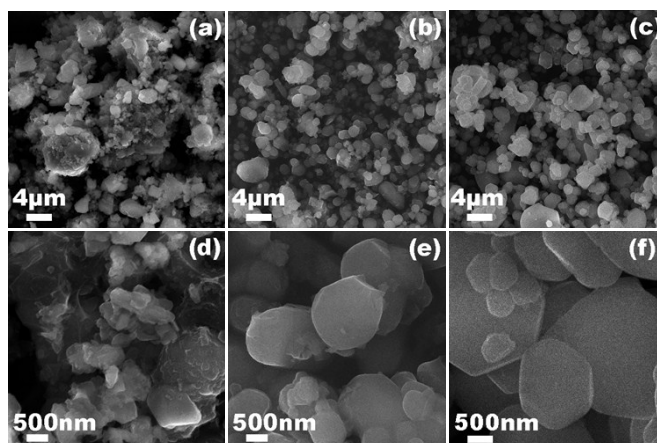


Figure S6. SEM images of the samples obtained at various $\text{NH}_4\text{F}/\text{Fe}(\text{acac})_3$ molar ratios of (a and d) 4:1, (b and e) 6:1 and (c and f) 8:1 at 200 °C for 2 h.

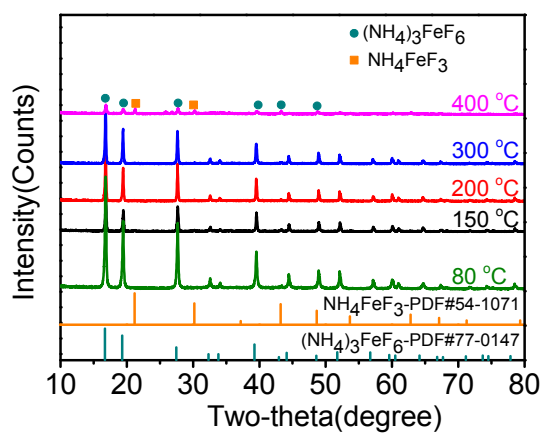


Figure S7. XRD pattern of the samples obtained at different reaction temperatures of 80, 150, 200, 300 and 400 °C with a $\text{NH}_4\text{F}/\text{Fe}(\text{acac})_3$ molar ratio of 8:1.

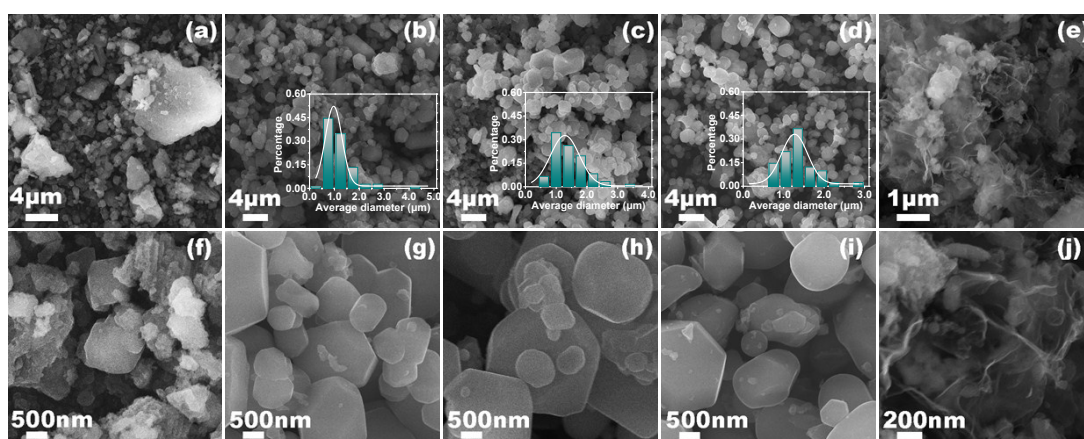


Figure S8. SEM images of the samples obtained at different reaction temperatures (a and f) 80, (b and g) 150, (c and h) 200, (d and i) 300 and (e and j) 400 °C with a $\text{NH}_4\text{F}/\text{Fe}(\text{acac})_3$ molar ratio of 8:1. (Inset: corresponding to the particles size distribution of the samples.)

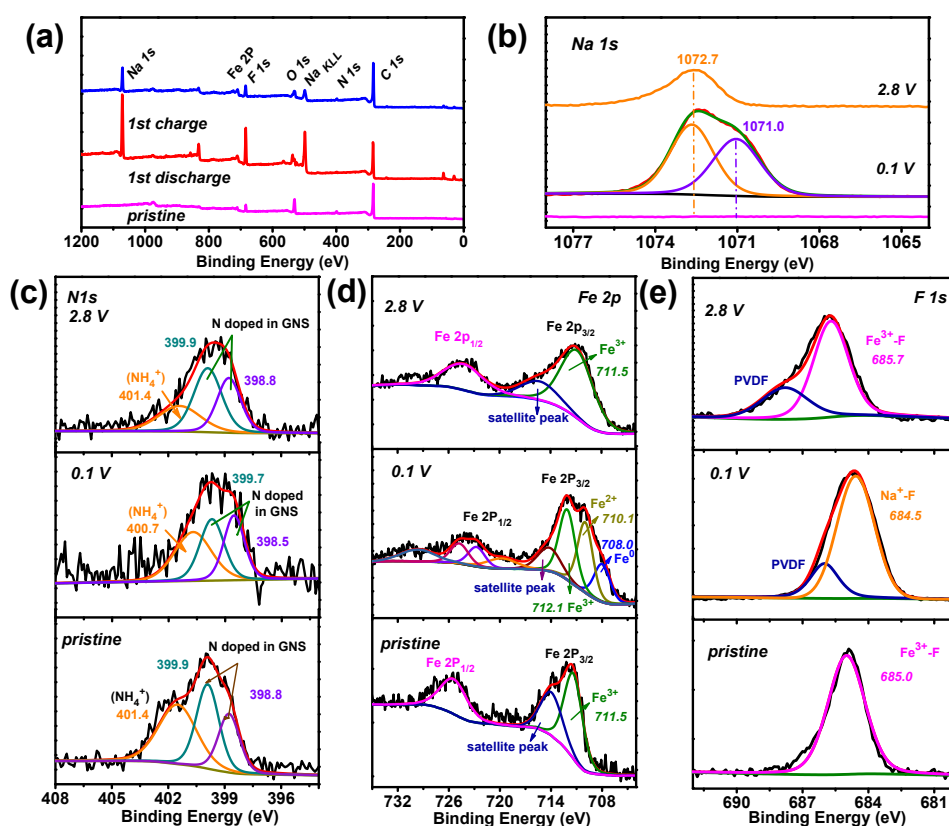


Figure S9. (a) XPS survey spectra, (b) Na1s, (c) N1s, (d) Fe2p and (e) F1s spectra of pristine $(\text{NH}_4)_3\text{FeF}_6/\text{GNS}$, and $(\text{NH}_4)_3\text{FeF}_6/\text{GNS}$ electrodes after discharging to 0.1 V and charging to 2.8 V in the first cycle, respectively.

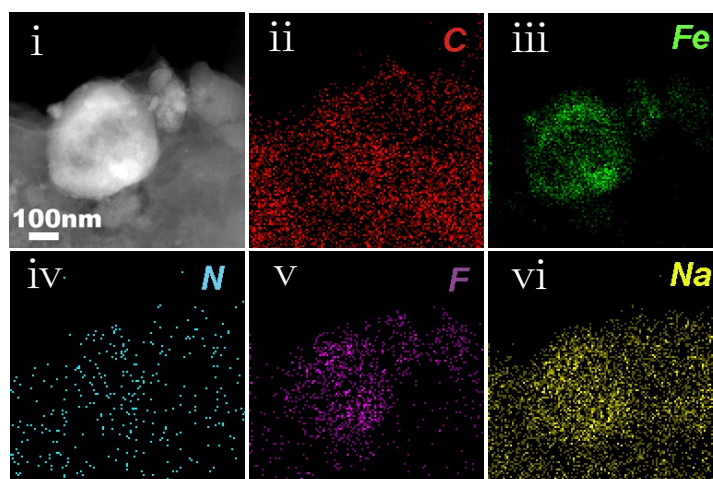


Figure S10. (i) STEM images of $(\text{NH}_4)_3\text{FeF}_6/\text{GNS}$ electrode after discharging to 0.1 V in the first cycle and corresponding elemental mappings of C (ii), Fe (iii), N (iv), F (v), Na (vi).

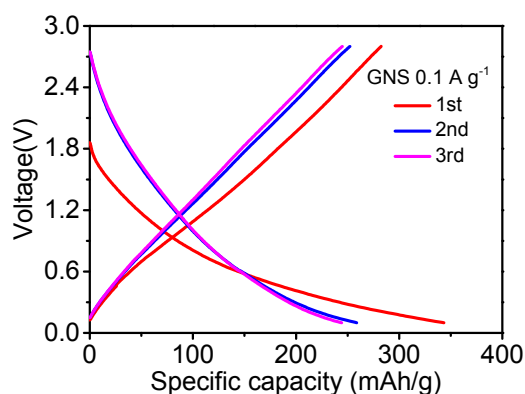


Figure S11. The initial three charge/discharge curves of GNS at 0.1 A g^{-1} .

The first reversible capacities of $(\text{NH}_4)_3\text{FeF}_6/\text{GNS}$ and GNS are ca. $487.8 \text{ mA h g}^{-1}$ and $282.5 \text{ mA h g}^{-1}$ (Fig. S11). Therefore, the specific capacity contribution of GNS in the $(\text{NH}_4)_3\text{FeF}_6/\text{GNS}$ composite is 62.1 mA h g^{-1} (calculated by $282.5 \times 22.0\%$), and the specific capacity contribution of $(\text{NH}_4)_3\text{FeF}_6$ in the $(\text{NH}_4)_3\text{FeF}_6/\text{GNS}$ should be $425.7 \text{ mA h g}^{-1}$ (calculated by $487.8 - 62.1$). Therefore, the actual capacity of $(\text{NH}_4)_3\text{FeF}_6$ is ca. $545.7 \text{ mA h g}^{-1}$ (calculated by $425.7 / 78.0\%$).

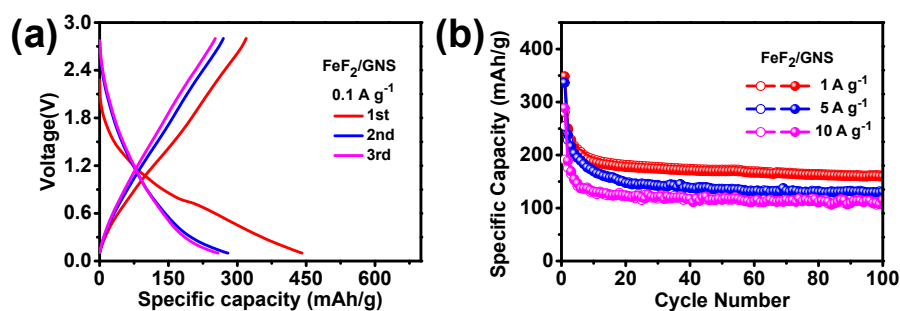


Figure S12. (a) initial three galvanostatic charge/discharge curves and (b) cycling performances of FeF_2/GNS .

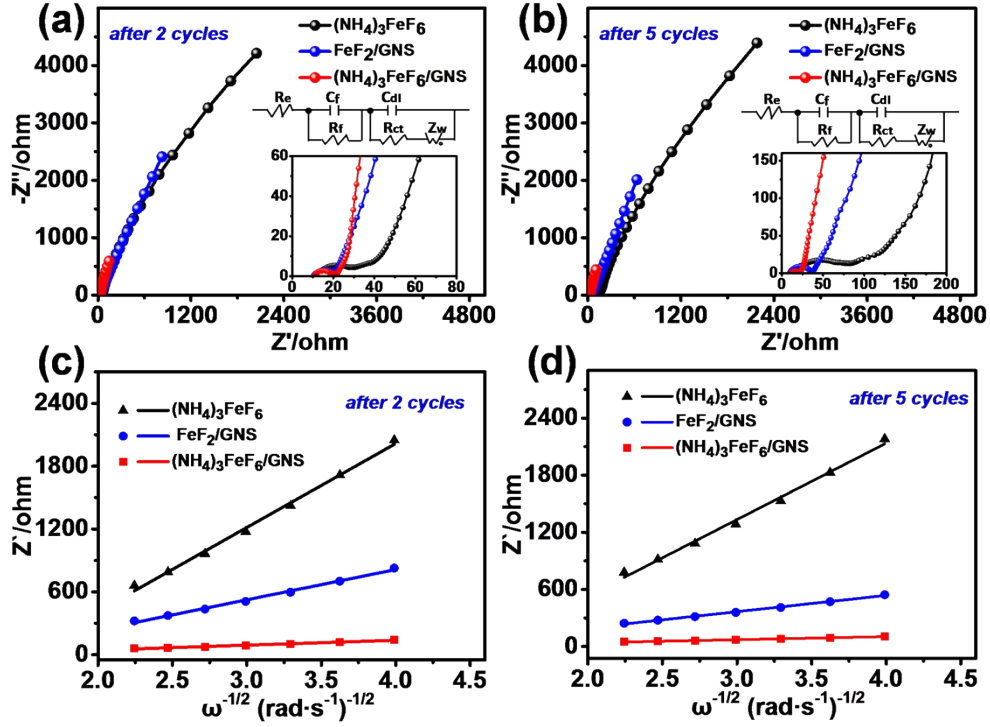


Figure S13. (a, b) Electrochemical impedance spectroscopy (EIS) after 2 cycles and 5 cycles at 0.1 A g^{-1} , (c, d) Warburg coefficient σ after 2 cycles and 5 cycles at low-frequency of pure $(\text{NH}_4)_3\text{FeF}_6$, FeF_2/GNS and $(\text{NH}_4)_3\text{FeF}_6/\text{GNS}$. (Inset: corresponding to equivalent circuit model for SIBs.)

Table S1. The fitting results of the EIS curves obtained by equivalent circuit.

The sample		R_e (Ω)	R_f (Ω)	R_{ct} (Ω)	σ ($\Omega \cdot \text{s}^{-1/2}$)	D ($\text{cm}^2 \cdot \text{s}^{-1}$)
$(\text{NH}_4)_3\text{FeF}_6$	After 2-cycles	14.13	8.35	5.98	801.311	3.21×10^{-17}
	After 5-cycles	15.42	11.76	26.41	803.124	3.21×10^{-17}
FeF_2/GNS	After 2-cycles	10.07	3.49	6.00	288.74	4.05×10^{-16}
	After 5-cycles	10.09	8.97	15.57	171.32	1.15×10^{-15}
$(\text{NH}_4)_3\text{FeF}_6/\text{GNS}$	After 2-cycles	11.33	4.53	3.01	47.211	3.13×10^{-13}
	After 5-cycles	11.63	4.72	3.26	32.043	6.80×10^{-13}

As shown in Fig. S13, the EIS curves of the pure $(\text{NH}_4)_3\text{FeF}_6$, FeF_2/GNS and $(\text{NH}_4)_3\text{FeF}_6/\text{GNS}$ were fitted by the equivalent circuit, which consist of a semicircle in high frequency region and a line in low frequency region. R_e is the electrolyte impedance, and R_f and C_f are the resistance and capacitance of the SEI layer formed on the surface of the electrodes, respectively. R_{ct} and C_{dl} are the charge-transfer resistance and double-layer capacitance. Z_w is the Warburg impedance. The sodium ion diffusion coefficient (D) can be calculated at low frequency with the Equation S1:

$$D = \frac{R^2 T^2}{2A^2 n^4 F^4 C^2 \sigma^2} \quad \text{Equation S1}$$

where R is the gas constant, T is the absolute temperature in experiment, A is the electrode surface area, n is the number of transferred electrons, F is Faraday's constant, C is the concentration

of sodium ion in anode electrode materials. σ is the Warburg coefficient, which was determined as the slope of Z' vs. $\omega^{-1/2}$ plots in the low-frequency region. The value of σ can be got by the Equation S2:

$$Z' = R_e + R_{ct} + \sigma\omega^{-1/2} \quad \text{Equation S2}$$

The EIS simulation results of the pure $(\text{NH}_4)_3\text{FeF}_6$ and $(\text{NH}_4)_3\text{FeF}_6/\text{GNS}$ are presented in Fig. S13 and Table S1.

The sodium ion diffusion coefficient (D) of pure $(\text{NH}_4)_3\text{FeF}_6$, FeF_2/GNS and $(\text{NH}_4)_3\text{FeF}_6/\text{GNS}$ are 3.21×10^{-17} , $4.05 \times 10^{-16} \text{ cm}^2 \text{ s}^{-1}$ and $3.13 \times 10^{-13} \text{ cm}^2 \text{ s}^{-1}$ after the 2th cycle, and 3.21×10^{-17} , $1.15 \times 10^{-15} \text{ cm}^2 \text{ s}^{-1}$ and $6.80 \times 10^{-13} \text{ cm}^2 \text{ s}^{-1}$ after 5th cycle, respectively.

Table S2. Electrochemical performance comparison for Na-ion storage performances of TMFs reported in the references.

Materials	Crystal structure	Voltage range	Initial reversible capacity	Cycle performance	Rate performance	Ref
CoF_2	Rutile-type	0.01-3.0 V	190 mA h g ⁻¹ at 553 mA g ⁻¹	40.7 mA h g ⁻¹ at 553 mA g ⁻¹ after 30 cycles	—	1
$\text{TiO}_{0.9}(\text{OH})_{0.3}\text{F}_{12} \cdot 0.59\text{H}_2\text{O}$	Hexagonal-tungsten-bronze-type	0.5-2.9 V	150 mA h g ⁻¹ at 25 mA g ⁻¹	100 mA h g ⁻¹ at 25 mA g ⁻¹ after 115 cycles	160 mA h g ⁻¹ at 25 mA g ⁻¹ 130 mA h g ⁻¹ at 50 mA g ⁻¹ 120 mA h g ⁻¹ at 75 mA g ⁻¹ 100 mA h g ⁻¹ at 125 mA g ⁻¹	2
$\text{SnF}_2@\text{C}$	Like-rutile-type	0.01-2.0 V	563 mA h g ⁻¹ at 0.05 C	337 mA h g ⁻¹ at 0.05 C after 50 cycles	490 mA h g ⁻¹ at 0.05 C 384 mA h g ⁻¹ at 0.1 C 329 mA h g ⁻¹ at 0.2 C 288 mA h g ⁻¹ at 0.5 C 191 mA h g ⁻¹ at 1C	3
NaF-Ti	—	0.01-2.5 V	45 $\mu\text{Ah cm}^{-2}$ at 2 $\mu\text{A cm}^{-2}$	—	4.1 $\mu\text{Ah cm}^{-2}$ at 2 $\mu\text{A cm}^{-2}$ 1.7 $\mu\text{Ah cm}^{-2}$ at 8 $\mu\text{A cm}^{-2}$ 1.2 $\mu\text{A cm}^{-2}$ at 12 $\mu\text{A cm}^{-2}$ 0.7 $\mu\text{A cm}^{-2}$ at 20 $\mu\text{A cm}^{-2}$	4
$\text{KNb}_2\text{O}_5\text{F}$	Tetragonal-tungsten-bronze-type	0.1-3.0 V	170-180 mA h g ⁻¹ at 0.1 C	100-110 mA h g ⁻¹ at 0.1 C after 140 cycles	-90 mA h g ⁻¹ at 0.5 C 60 mA h g ⁻¹ at 1 C -30 mA h g ⁻¹ at 5 C	5
$\text{NH}_4\text{FeF}_6/\text{GNS}$	Perovskite	0.1-2.8 V	504 mA h g ⁻¹ at 0.05 A g ⁻¹	175 mA h g ⁻¹ at 0.2 A g ⁻¹ after 100 cycles 117 mA h g ⁻¹ at 0.5 A g ⁻¹ after 100 cycles	211 mA h g ⁻¹ at 0.2 A g ⁻¹ 153 mA h g ⁻¹ at 0.5 A g ⁻¹ 113 mA h g ⁻¹ at 1.0 A g ⁻¹ 76 mA h g ⁻¹ at 2.0 A g ⁻¹	6
FeF_2/GNS	Rutile-type	0.1-2.8 V	319.3 mA h g ⁻¹ at 0.1 A g ⁻¹	160.2 mA h g ⁻¹ at 1.0 A g ⁻¹ after 100 cycles 130.3 mA h g ⁻¹ at 5.0 A g ⁻¹ after 100 cycles	—	This work
$(\text{NH}_4)_3\text{FeF}_6/\text{GNS}$	Diperovskite	0.1-2.8 V	487.8 mA h g ⁻¹ at 0.1 A g ⁻¹	276.9 mA h g ⁻¹ at 1.0 A g ⁻¹ after 100 cycles 177.4 mA h g ⁻¹ at 5.0 A g ⁻¹ after 100 cycles	287.3 mA h g ⁻¹ at 1.0 A g ⁻¹ 257.8 mA h g ⁻¹ at 2.0 A g ⁻¹ 219.4 mA h g ⁻¹ at 5.0 A g ⁻¹ 180.6 mA h g ⁻¹ at 10.0 A g ⁻¹	This work

References

- 1 J. Tan, L. Liu, S. Guo, H. Hu, Z. Yan, Q. Zhou, Z. Huang, H. Shu, X. Yang and X. Wang, *Electrochim. Acta*, 2015, **168**, 225-233.
- 2 B. Li, Z. Gao, D. Wang, Q. Hao, Y. Wang, Y. Wang and K. Tang, *Nanoscal Res. Lett.*, 2015, **10**, 409.
- 3 G. Ali, J.-H. Lee, S. H. Oh, H.-G. Jung and K. Y. Chung, *Nano Energy*, 2017, **42**, 106-114.
- 4 W.-M. Liu, Q. Sun and Z.-W. Fu, *Electrochem. Commun.*, 2013, **27**, 156-159.
- 5 Y. Han, M. Yang, Y. Zhang, J. Xie, D. Yin and C. Li, *Chem. Mater.*, 2016, **28**, 3139-3147.
- 6 M. Kong, K. Liu, J. Ning, J. Zhou and H. Song, *J. Mater. Chem. A*, 2017, **5**, 19280-19288.